Secondary Flow over Surfaces with Spanwise Heterogeneity

D. D. Wangsawijaya[1], **C. M. de Silva**[1], **R. Baidya**[1], **D. Chung**[1], **I. Marusic**[1], **N. Hutchins**[1]

[1]Department of Mechanical Engineering
The University of Melbourne, Victoria 3010, Australia

Abstract

Surfaces with heterogeneous roughness are known to alter the behaviour of canonical turbulent boundary layers. In the case where roughness varies in the spanwise direction, the turbulent boundary layer is modified by secondary flows in the form of counter-rotating streamwise roll modes. Previous studies on various spanwise heterogeneity models have shown that the behaviour of these secondary flows is determined by the type, spacing, and the width of the roughness elements. To examine this further, we here conduct a series of hot-wire anemometry measurements over surfaces with strips of spanwise heterogeneous roughness, where the ratio of the roughness strip width Λ and the spanwise-averaged boundary layer thickness $\overline{\delta}$ varies in the range of $\Lambda/\overline{\delta} = 0.32$–$3.63$. Our results show that the secondary flow appears to amplify a particular energetic mode in the outer layer ($z/\overline{\delta} \approx 0.5$), as evidenced by a peak in the 1-D energy spectra at this wall-normal location for all test cases. This behaviour is observed to be the strongest at $\Lambda/\overline{\delta} \approx 1$. In the cases where $\Lambda/\overline{\delta}$ approaches its limit ($\Lambda/\overline{\delta} \gg 1$ or $\Lambda/\overline{\delta} \ll 1$), the magnitude of this spectral peak diminishes and the size and location of the secondary flow are limited by either the spanwise extent of Λ or the height of $\overline{\delta}$. Outside the region affected by the secondary flow, the behaviour of surfaces with spanwise heterogeneity appears to approach that of homogeneous flow.

Introduction

Although engineers have an extensive set of tools for predicting wall-bounded turbulent flows over homogeneous surface roughness, the same cannot be said for cases where roughness properties vary extensively along the surface. This latter case is more typical in engineering applications and the natural environment, as seen in atmospheric flow over forest interfaces, urban cities, biofouling on ship hulls, rivet rows and panel joints on aircraft skin, et cetera.

For this study, we consider the case where heterogeneous roughness is distributed along the spanwise direction. For such a surface, interaction of the turbulence and surface heterogeneity induces secondary flows in the form of counter-rotating streamwise roll modes embedded within the boundary layer [1]. Hinze [3] attributes these roll modes to the transport of highly turbulent flow from a region where production exceeds dissipation to adjacent regions in the spanwise direction where dissipation locally exceeds production, a necessity for maintaining energy balance. This results in a downward flow above high shear stress region and upward above low shear stress regions.

Existing works on spanwise heterogeneity due to imposed wall shear stress variation, namely [3] and [11], showed that time-averaged streamwise velocity is lower (with respect to its spanwise averaged value) over the low shear stress regions at a given wall height. A more recent work by Chung, Monty, & Hutchins [2] showed that the opposite situation could also happen, with low shear stress regions exhibiting higher streamwise velocity at $\Lambda/\delta = 6.28$, yet switching to lower velocity at $\Lambda/\delta = 1.57$, where δ is the half-height of the channel. For this type of spanwise heterogeneity, upwelling generally occurs
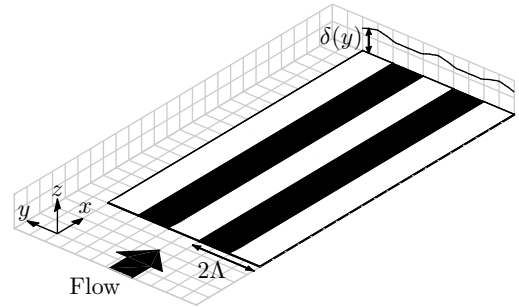
Figure 1: Illustration of spanwise heterogeneous roughness model. The white and black patches correspond to strips of cardboard and sandpaper, respectively. Solid line indicates the spanwise variation of boundary layer thickness, $\delta(y)$.

above the low shear stress regions. On the other hand, both up-welling and downwelling are observed above the roughness elements for ridge-type roughness, where the roughness elements have a virtual origin that is substantially elevated above that of the smooth surface. Yang & Anderson [12] showed reversal in the secondary flow direction on ridge-type roughness from downwelling above roughness elements at $s/\delta \geq 1$ to upwelling for $s/\delta < 1$, where s is the spacing between roughness elements. Conversely, other studies on ridge-type roughness by Vanderwel & Ganapathisubramani [10] for $s/\overline{\delta} = 0.3$–$1.76$ and Medjnoun, Vanderwel, & Ganapathisubramani [7] for $s/\overline{\delta} = 0.8$–$3.2$ have suggested that upwelling always occurs above roughness elements within these $s/\overline{\delta}$ ranges. Despite these differences and the influence of ridge width [5], all of these works have shown similar limiting cases. When the roughness spanwise width is very large ($\Lambda/\delta = 6.28$ [2], $s/\overline{\delta} > 3.2$ [7]), the boundary layer away from the stress jump behaves according to its local shear stress and outer-layer similarity is recovered. Meanwhile, when the spanwise width is very small ($\Lambda/\delta = 0.39$ [2], $s/\delta \ll 1$ [12]), the boundary layer becomes spanwise homogeneous. Between the two limits ($\Lambda/\delta = 1.57$ [2], $1 \leq s/\delta \leq 2$ [12]), the secondary flow fills the entire boundary layer, outer layer similarity is not observed, and the flows are fully heterogeneous in spanwise direction.

While the effect of spacing on the secondary flow and mean velocity profile has been investigated extensively, its impact on the energy spectra as a function of wall-height is largely unexplored. For example, the presence of a secondary spectral peak in the outer layer, possibly due to secondary flow, was mentioned in [7] for ridge-type roughness and [8] for converging-diverging riblets (which arranges the flow in such way that counter-rotating streamwise secondary flows are generated). In this study, we further examine the effect of the secondary flow on the energy spectra of the turbulent boundary layer over surfaces for various $\Lambda/\overline{\delta}$.

Experiments

The measurements are performed in a zero pressure gradient, open return boundary layer wind tunnel in the Walter Basset

Case	Λ (mm)	$\overline{\delta}$ (mm)	$\Lambda/\overline{\delta}$	Re_x $\times 10^{-6}$	$Re_{\overline{\delta}}$ $\times 10^{-4}$	$Re_{\overline{\theta}}$
SR250	250	68.8	3.63	3.91	6.72	9090
SR160	160	70.0	2.28	3.91	6.84	9200
SR100	100	69.7	1.43	3.92	6.83	9060
SR50	50	77.1	0.65	3.91	7.54	9110
SR25	25	77.6	0.32	3.86	7.49	9990

Table 1: Summary of spanwise heterogenous roughness cases.

Aerodynamic Laboratory at the University of Melbourne. The test section has the dimension of 6.7 m × 0.94 m × 0.38 m. The turbulent boundary layer is tripped by a strip of P-40 grit sandpaper glued to the inlet of the test section.

For the present experiments, the spanwise heterogeneous roughness surfaces, shown in figure 1, are constructed from strips of P-36 grit sandpaper ("rough" patch) and 2 mm-thick cardboard ("smooth" patch) of equal width Λ, which are laid in a spanwise-alternating pattern to cover 5.6 m-long section of the wind tunnel from the boundary layer trip. This arrangement provides a wall surface that is composed of spanwise periodic rough and smooth patches of 2Λ wavelength. The thickness of the cardboard strips is designed to minimise variation in the virtual origin between rough and smooth strips. Five such surfaces with varying Λ are constructed in order to obtain a range of $\Lambda/\overline{\delta}$ from 0.32 to 3.63, where $\overline{\delta}$ corresponds to the mean 98% boundary layer thickness averaged over one half-wavelength of the surface. Measurements are carried out at a constant freestream velocity $U_\infty \approx 15$ ms^{-1}, 4 m downstream of the turbulent boundary layer trip.

Hot-wire Anemometry

Two sets of hot-wire measurements over spanwise heterogeneous roughness models are performed for each case in table 1. The first is a wall-normal measurement at 40 logarithmically-spaced wall-normal locations over the center of the smooth patch to obtain the near-wall turbulent boundary layer. The second is a measurement over a spanwise wall-normal grid, in which the hot-wire probe obtains turbulent boundary layer profiles with 30 logarithmically spaced wall-normal locations at 11 (case SR25-SR160) and 15 (case SR250) spanwise locations over one half-wavelength Λ of the surface. The measurement starts from the midpoint of a smooth patch and ends at the middle of the adjacent rough patch.

All hot-wire measurements are carried out using a modified Dantec 55P05 single-sensor boundary layer probe. The sensor is formed from a platinum wire with 5 μm diameter and approximately 1 mm etched length, which is equivalent to 36 viscous units for the smooth wall boundary layer. The anemometer used in this study is an in-house constant temperature anemometer (MUCTA) with a fixed overheat ratio of 1.8. The output signal from the hot-wire is sampled at 30 kHz and low-pass filtered at the cut-off frequency of 15 kHz. Sampling time is set to maintain turnover rate $TU/\delta \geq 20,000$ and thus allows the convergence of turbulence energy spectra [4].

Results

The 1-D energy spectra of the streamwise velocity fluctuations Φ_{uu} are calculated as a function of wall-normal and spanwise location. The relationship between velocity fluctuations and the energy spectra is given by

$$\overline{u'^2} = \int_0^\infty \Phi_{uu}\mathrm{d}(k_x) \qquad (1)$$
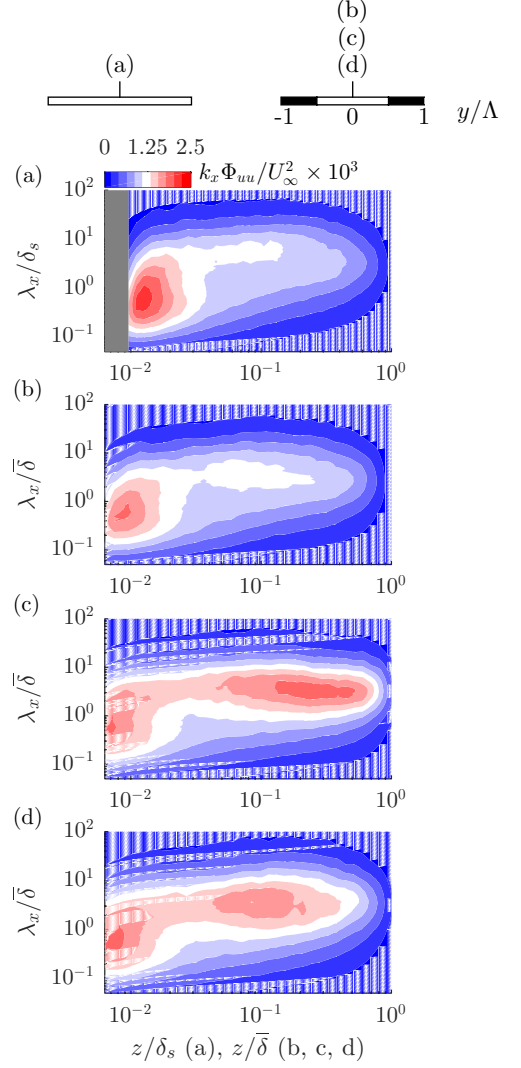
Figure 2: Contour of premultiplied streamwise energy spectra of (a) a reference smooth wall and midpoint of the smooth patch ($y/\Lambda = 0$, see legend) for case: (b) SR250 ($\Lambda/\overline{\delta} = 3.63$), (c) SR50 ($\Lambda/\overline{\delta} = 0.65$), (d) SR25 ($\Lambda/\overline{\delta} = 0.32$). Near-wall data are not available in the grey-shaded area; δ_s is the 98% boundary layer thickness of the smooth wall.

where k_x is the wavenumber. We assume that Taylor's hypothesis holds [9], which permits time-series data conversion to space using $\Delta x = -U_c\Delta t$. Here, the convection velocity U_c is the local mean streamwise velocity U at each wall-normal location. Based on this definition, streamwise wavelength is defined as $\lambda_x = U/f$ and the wavenumber equals $k_x = 2\pi/\lambda_x$. For the present experiments, no attempt is made to measure drag. Therefore, the energy spectra are normalized by the freestream velocity U_∞^2.

The contours of premultiplied energy spectra $k_x\Phi_{uu}$ at the midpoint of the smooth patch ($y/\Lambda = 0$) for a few select cases from large to small $\Lambda/\overline{\delta}$ are shown in figure 2(b-d). The results reveal that the large scales in the logarithmic and outer region tend to be more energized as $\Lambda/\overline{\delta}$ decreases. More specifically, the energy spectra in the outer region peak at $\Lambda/\overline{\delta} = 0.65$ (figure 2b), thereafter reduce in magnitude at smaller $\Lambda/\overline{\delta}$.

For all spanwise heterogeneous cases, comparisons are made with the energy spectra of a reference smooth wall at a similar Re_x ($Re_{\delta_s} = 5.62 \times 10^4, Re_{\theta_s} = 7320$) in figure 2(a). Note that
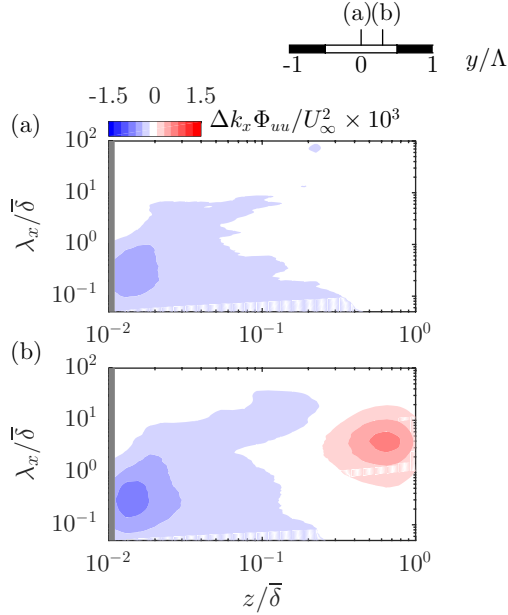
Figure 3: Difference between energy spectra of SR250 case and a smooth wall: (a) midpoint of a smooth patch ($y/\Lambda = 0$, see legend) and (b) near rough-to-smooth interface ($y/\Lambda = 0.3$).

Figure 4: Difference between energy spectra of SR25 case and a smooth wall: (a) midpoint of a smooth patch ($y/\Lambda = 0$, see legend) and (b) midpoint of the adjacent rough patch ($y/\Lambda = 1$). Dashed line is $z/\overline{\delta} = 0.32$.

Figure 5: Maximum difference between energy spectra of all spanwise heterogeneous roughness cases and a smooth wall: ●, midpoint of a smooth patch ($y/\Lambda = 0$) and ●, all spanwise measurement locations over the smooth patch. Dashed line is the maximum difference between a rough wall constructed from a P-36 grit sandpaper and a smooth wall.

wall height z and λ_x in figure 2(a) are normalized by the smooth wall boundary layer thickness, while the remaining subplots are normalized by $\overline{\delta}$. At first glance, the energy contained in the near-wall region appears to be consistently lower than that of the smooth wall for all cases. At the highest $\Lambda/\overline{\delta}$ in figure 2(b), the spectra exhibit similar characteristics to those of the smooth wall, with the exception of a slightly lower energy at the near-wall peak and a slightly expanded outer peak due to the large scales in the logarithmic region. Similarity with the reference smooth wall, however, does not extend to cases with smaller $\Lambda/\overline{\delta}$ (figure 2c-d).

In order to better quantify the behaviour of the spectral peak in the outer region, figure 3 shows the difference between premultiplied energy spectra of the smooth patch of the heterogeneous roughness and the smooth wall, $\Delta k_x \Phi_{uu}$, for the SR250 case ($\Lambda/\overline{\delta} = 3.63$). Note that the spectral difference is presented as a function of z and λ_x normalized by $\overline{\delta}$. Figure 3(a) shows that the energy spectra at the center of the smooth strip, $y/\Lambda = 0$, approach those of the smooth wall. However, we observe that an over-energized outer peak still exists for this surface closer to the smooth-to-rough interface ($y/\Lambda = 0.3$), as shown in figure 3(b). This result suggests that the secondary flow leads to an over-energized outer peak in the energy spectra, but its precise location and size are a function of $\Lambda/\overline{\delta}$. We note that, as proposed by Hinze [3], the secondary flow occurs due to the production-dissipation imbalance, which would be expected to occur above the rough-to-smooth interface. Moreover, the secondary flow is embedded within the turbulent boundary layer and so its size (or diameter of the roll modes) is likely to be confined by boundary layer thickness when $\Lambda > \overline{\delta}$. Further from the rough-to-smooth interface, the surface behaves according to its local shear stress, i.e. the smooth patch becomes increasingly similar to a smooth wall. This finding is in line with Medjnoun *et al.* [7], who shows that a velocity profile far removed from the secondary flow aproaches the smooth wall at $s/\overline{\delta} = 3.2$. Future works are planned at even larger $\Lambda/\overline{\delta}$ to understand this behaviour further.

A prominent outer peak at the center of the smooth strip is ob-

served when $\Lambda/\overline{\delta} \approx 1$, as shown in figure 2(c). At this ratio, the outer peak has the highest energy of all the case tested, while the small scales in the near-wall region has lower energy and the larger scales ($\lambda_x \approx 1$–$10\overline{\delta}$) are energized across the wall height. It would appear that when $\Lambda/\overline{\delta} \approx 1$, a certain streamwise mode is excited, as shown by the strong broad outer peak in figure 2(c) (SR50, $\Lambda/\overline{\delta} = 0.65$) at $\lambda_x \approx 3$–$4\overline{\delta}$. In the physical sense, this strong outer peak suggests that the streamwise roll-modes are not a constant time-invariant feature. Instead, the location of the low- and high-speed regions vary relative to the geometry of spanwise heterogeneous roughness as the roll-modes meander [6].
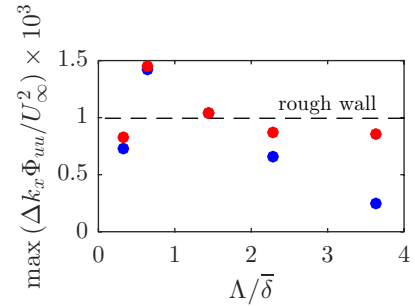
It is worth noting that an outer peak was also observed by Nugroho, Hutchins, and Monty [8] at $\Lambda/\overline{\delta} = 1.42$ over the converging region of converging-diverging riblets, which corresponds to the upwelling. Our results indicate similar behaviour for all cases; there is an outer peak located *somewhere* over the smooth patch, where upwelling generally occurs, but the precise spanwise location of the secondary flow seems to vary with

$\Lambda/\overline{\delta}$. Other work in ridge-type roughness [7] has reported an outer peak at two spanwise locations: the valley between two roughness elements for $s/\overline{\delta} = 0.8$ and somewhere between the valley and a roughness element for $s/\overline{\delta} = 1.7$. The upwelling, however, generally occurs above the roughness elements for the range of $s/\overline{\delta}$ tested in their study. This raises a question for the current spanwise heterogeneous roughness model on the effect of the secondary flow on the energy distribution above the rough patch, where downwelling generally occurs, which we plan to investigate in the future.

As $\Lambda/\overline{\delta}$ decreases further, the outer peak vanishes, replaced with higher energy across almost all wavelength and wall-normal height (figure 4). When $\Lambda < \overline{\delta}$, the secondary flow has a wall-normal extent that is restricted to $z < \Lambda$. Figure 4 shows such a scenario where $\Lambda/\overline{\delta} = 0.32$ and hence the secondary flow is confined within $z/\overline{\delta} < 0.32$, as shown by the dashed line. To the right hand side of this line, the energy spectra at the midpoint of the smooth patch ($y/\Lambda = 0$, figure 4a) are comparable to those at the center of the to rough patch ($y/\Lambda = 1$, figure 4b), both with higher energy than the reference smooth wall. This shows that as $\Lambda/\overline{\delta} \ll 1$, the surface roughness gradually becomes spanwise homogeneous, with the exception of the near-wall region ($z \lesssim \Lambda$) that is affected by the secondary flow.

Figure 5 summarizes the maximum difference between the energy spectra of the smooth patch and the smooth wall for all the test cases in table 1. For the red symbols, the displayed maximum difference is the maximum from all available spanwise locations over the smooth patch. The trend suggests that a meandering, or time-varying behaviour, of the secondary flow becomes maximum at a certain wall height and streamwise wavelength at $\Lambda/\overline{\delta} \approx 1$. This corresponds to the case where the secondary flows would be expected to fill the boundary layer. In the other cases, the maximum energy spectra difference tends to be constant and remains lower than those of a rough wall constructed entirely from the same sandpaper, regardless of $\Lambda/\overline{\delta}$ and spanwise location of the secondary flows. The magnitude of the maximum difference at the middle of a smooth patch (blue symbols), however, gradually diminishes and approaches the smooth wall as $\Lambda/\overline{\delta}$ increases. This is expected, since the center of the smooth patch is further and further from the secondary flows (and their time-varying behaviour) as $\Lambda/\overline{\delta}$ becomes large.

Conclusions

This study examines the turbulent boundary layer over surfaces with spanwise heterogenous roughness. To this end, a set of hot-wire anemometry measurements is conducted over such surfaces with various roughness width to boundary layer thickness ratios $\Lambda/\overline{\delta} = 0.32\text{--}3.63$. One-dimensional streamwise energy spectra taken at several measurement locations in the spanwise direction reveal that the secondary flows induced by spanwise heterogeneous roughness leads to an outer peak in the energy spectra contour. Furthermore, its location and size appear to be a function of $\Lambda/\overline{\delta}$. The strongest outer peak in the energy spectra is observed at $\Lambda/\overline{\delta} \approx 1$, close to the midpoint of the smooth patch, where upwelling occurs. This peak is thought to be related to an instability and strong meandering tendency of the secondary flow at these wavelengths. The peak is not as strong for the two limiting cases: $\Lambda/\overline{\delta} \gg 1$ and $\Lambda/\overline{\delta} \ll 1$. For these limits, the size and location of the secondary flow are limited by either Λ or $\overline{\delta}$. For $\Lambda/\overline{\delta} \gg 1$, it is predicted that the spanwise heterogeneous surface behaves according to its local shear stress with the exception of the region near the smooth-to-rough interface, where the secondary flow is located. For $\Lambda/\overline{\delta} \ll 1$, the secondary flow is confined to the near-wall region ($z \lesssim \Lambda$) and the surface becomes spanwise homogeneous above this region.

References

[1] Bradshaw, P., Turbulent secondary flows, *Annu. Rev. Fluid Mech.*, **19**, 1987, 53–74.

[2] Chung, D., Monty, J. P. and Hutchins, N., Similarity and structure of wall-turbulence with lateral wall shear stress variations, *J. Fluid Mech.*, **847**, 2018, 591–613.

[3] Hinze, J. O., Secondary currents in wall turbulence, *Phys. Fluid*, **10**, 1967, S122.

[4] Hutchins, N., Nickels, T. B., Marusic, I. and Chong, M. S., Hot-wire spatial resolution issues in wall-bounded turbulence, *J. Fluid Mech.*, **635**, 2009, 103–136.

[5] Hwang, H. G. and Lee, J. H., Secondary flows in turbulent boundary layers over longitudinal surface roughness, *Phys. Rev. Fluids*, **3**, 2018, 014608.

[6] Kevin, Monty, J. P., Bai, H. L., Pathikonda, G., Nugroho, B., Barros, J. M., Christensen, K. T. and Hutchins, N., Cross-stream stereoscopic particle image velocimetry of a modified turbulent boundary layer over directional surface pattern, *J. Fluid Mech.*, **813**, 2017, 412–435.

[7] Medjnoun, T., Vanderwel, C. and Ganapathisubramani, B., Characteristics of turbulent boundary layers over smooth surfaces with spanwise heterogeneity, *J. Fluid Mech.*, **838**, 2018, 516–543.

[8] Nugroho, B., Hutchins, N. and Monty, J. P., Large-scale spanwise periodicity in a turbulent boundary layer induced by highly ordered and directional surface roughness, *Int. J. Heat Fluid Flow*, **41**, 2013, 90–102.

[9] Taylor, G. I., The spectrum of turbulence, *Proc. R. Soc. Lond. A*, **164**, 1938, 476–490.

[10] Vanderwel, C. and Ganapathisubramani, B., Effects of spanwise spacing on large-scale secondary flows in rough-wall turbulent boundary layers, *J. Fluid Mech.*, **774**, 2015, R2.

[11] Willingham, D., Anderson, W., Christensen, K. T. and Barros, J. M., Turbulent boundary layer flow over transverse aerodynamic roughness transitions: Induced mixing and flow characterization, *Phys. Fluid*, **26**, 2014, 025111.

[12] Yang, J. and Anderson, W., Numerical study of turbulent channel flow over surfaces with variable spanwise heterogeneities: topographically-driven secondary flows affect outer-layer similarity of turbulent length scales, *Flow Turbul. Combust.*, **100**, 2018, 1–17.